Experimental and theoretical $(e,2e)$ ionization cross sections for a hydrogen target at 75.3 eV incident energy in a coplanar asymmetric geometry

Junfang Gao,[a] D. H. Madison, and J. L. Peacher
Department of Physics, University of Missouri–Rolla, Rolla, Missouri 65409

Andrew James Murray and Martyn J. Hussey
School of Physics and Astronomy, Schuster Laboratory, The University of Manchester, Manchester M13 9PL, United Kingdom

(Received 29 March 2006; accepted 5 April 2006; published online 16 May 2006)

Very recently it was shown that the molecular three-body distorted wave (M3DW) approach gives good agreement with the shape of the experimental data for electron-impact ionization of H_2 in a coplanar symmetric geometry, providing the incident electrons have an energy of 35 eV or greater. One of the weaknesses of these studies was that only the shape of the cross section could be compared to experiment, since there was no absolute or relative normalization of the data. Here we report a joint experimental/theoretical study of electron-impact ionization of H_2 in a coplanar *asymmetric* geometry where the energy of the incident electron was fixed, and different pairs of final state electron energies were used. In this case, the experimental data can be normalized such that only one renormalization factor is required. It is shown that the M3DW is pretty good in agreement with experiment. However, a better treatment of polarization and exchange between the continuum and bound state electrons is required before quantitative agreement between experiment and theory is achieved. © *2006 American Institute of Physics*. [DOI: 10.1063/1.2200339]

I. INTRODUCTION

For the last two decades, high energy electron-impact ionization of atoms or molecules has been used to probe the details of molecular structures.[1] For sufficiently high incident electron energies (keV), the plane wave impulse approximation (PWIA) is successful, and so may be used to relate the experimentally determined cross sections to the momentum space wave function for the active electron which is ejected during ionization. More recently, low to intermediate incident-energy $(e,2e)$ results have been reported for relatively simple molecular systems.[2,3] For these cases the PWIA is no longer valid since the dynamics of the ionization collision become important. In these energy regimes, it is therefore necessary to apply more sophisticated models to accurately emulate experimental data.

Electron-impact ionization of the hydrogen molecule has often been discussed in text books[4,5] and in several journal articles,[6–18] since this is the simplest molecular system that can be easily studied both theoretically and experimentally. Early studies of the fully differential cross section (FDCS) for H_2 date back to 1973, when McCarthy[6] calculated the $(e,2e)$ relative differential cross section using the eikonal approximation, and Weigold *et al.*[7] performed the first experimental measurements on this target. In 1975, Dey *et al.*[8] studied the momentum space wave function for H_2 and compared their results with the Compton profile. In 1977 Weigold *et al.*[9] determined that the triple differential cross section for ionization of excited H_2 is very sensitive to electron correlation effects in the ground state. Additional measurements were performed in the early 1980s by Van Wingerden *et al.*,[10] Migdall *et al.*,[11] and Leung and Brion.[12] In 1989 absolute triple differential cross sections from H_2 were measured by Chérid *et al.*[13] Robicheaux[14] calculated the differential cross sections analytically for electron ionization of H_2^+ in 1996 using a spheroidal coordinate system, and Monzani *et al.*[15] reported a distorted wave Born approximation (DWBA) calculation of double and triple differential cross sections for electron ionization of H_2 in 1999. In this model, distorted waves were generated using the Schwinger variational iterative method.

In 2001 Weck *et al.*[16] proposed the two-effective center (TEC) approximation for ionization of H_2 by fast electron impact, and in 2002 Stia *et al.*[17] used the molecular Brauner-Briggs-Klar (MBBK) approximation to study $(e,2e)$ cross sections for H_2. Recently Murray[3] reported new coplanar symmetric measurements for ionization of H_2 in the intermediate to low energy range, and Gao *et al.*[18] used the distorted wave impulse approximation with orientation averaged molecular orbitals (DWIAOA) and the molecular three-body distorted wave (M3DW) approximation to examine both high (keV) and low (50 eV) incident-energy electron-impact ionization of H_2.

At low incident energies, the M3DW results of Gao *et al.*[18] agree reasonably well with experimental data for coplanar symmetric scattering from the Manchester group,[3] which were taken at incident energies ranging from 10 to 40 eV above the ionization threshold. Since the experimental data were not measured on an absolute scale, only the

[a]Electronic mail: jgzm6@umr.edu

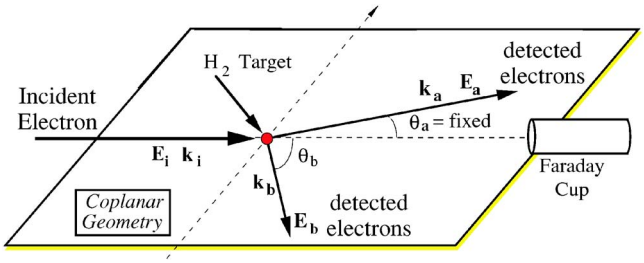

FIG. 1. The experimental coplanar asymmetric geometry used for the present studies. For details, see text.

shape of the theoretical results could be tested at each energy, with no guidance as to the relative magnitudes of the calculated cross sections.

To facilitate a more robust comparison between theory and experiment, it was therefore decided to take measurements at an incident energy where the model has proven to be more accurate and in an energy regime where the experimental apparatus could operate. The $(e,2e)$ spectrometer at Manchester was designed for low to intermediate energy regime studies, and so this restricts the possible incident energies that can be used. As comparison between theory and experiment proved to be most accurate at higher energies in the coplanar *symmetric* case, it was decided to use an incident energy of 75.3 eV (60 eV above the ionization threshold of 15.3 eV) and to adopt a coplanar *asymmetric* geometry for these new studies. In this case, one of the electron detectors was fixed at a forward angle θ_a, and the second detector moved around the scattering plane through angles θ_b, as shown in Fig. 1.

In contrast to conventional asymmetric scattering studies, it was decided to measure the cross sections for a range of outgoing electron energies (E_a,E_b) while keeping the incident energy fixed. This configuration had the advantage that the interaction region between the incident electron beam and the target gas beam remained the same throughout data collection, in contrast to the coplanar symmetric studies of Ref. 3 which used different incident electron beam energies. As such, it is more straightforward to estimate relative cross sections between the data by considering the effects of the electrostatic lenses used in the electron detectors.

In this paper, data for the ionization of H_2 are presented for a coplanar asymmetric geometry at a fixed incident electron energy of 75.3 eV, where the energy of the fixed electron is varied from 58 to 10 eV. In addition to being able to test the shape of the theoretical cross sections for asymmetric scattering, the experimental data are normalized so that the relative magnitudes of the theoretical cross sections can also be evaluated. Absolute cross sections are not determined; however, the relative normalization of the results allows only one point to be adjusted when comparing experiment to theory for the complete set of data presented here.

Theoretically, orientation averaged molecular orbitals (OAMOs) are used to evaluate the T matrix in this model.[19–23] Both the DWIAOA and the M3DW approximation are used to calculate the FDCS. For coplanar symmetric scattering, it is not necessary to calculate both direct and exchange amplitudes since they are identical. For coplanar asymmetric scattering this is not the case, and so both amplitudes must be evaluated for low incident electron energies, as studied here. The exchange amplitude treats exchange between the two continuum electrons. For electron-atom scattering, it has been shown that exchange between the continuum electrons and passive *bound* electrons can also be important. This exchange effect is normally called exchange distortion (ED) since it changes (distorts) the continuum wave functions. In this paper, ED is included using the Furness-McCarthy approximation[24] which has been shown to be accurate for ionization of xenon by spin polarized electrons.[25,26]

a.u. are used throughout this paper unless noted otherwise.

II. THEORY

The M3DW approximation which is based on the OAMO (Ref. 23) has been presented in previous publications,[22] so only a brief overview will be presented here. The previous work did not include the exchange amplitude. If exchange is included, the M3DW FDCS is given by

$$\frac{d^5\sigma}{d\Omega_a d\Omega_b dE_b} = \frac{1}{(2\pi)^5}\frac{k_a k_b}{k_i}(|T_{\rm dir}|^2 + |T_{\rm exch}|^2 + |T_{\rm dir} - T_{\rm exch}|^2), \quad (1)$$

where $T_{\rm dir}$ and $T_{\rm exch}$ are the direct and exchange amplitudes:

$$T_{\rm dir} = \langle \chi_a^-(\mathbf{r}_1)\chi_b^-(\mathbf{r}_2)C_{\rm proj\text{-}eject}(|\mathbf{r}_1-\mathbf{r}_2|)|V - U_i|\phi_j^{\rm OA}(\mathbf{r}_2)\chi_i^+(\mathbf{r}_1)\rangle. \quad (2)$$

$$T_{\rm exch} = \langle \chi_a^-(\mathbf{r}_2)\chi_b^-(\mathbf{r}_1)C_{\rm proj\text{-}eject}(|\mathbf{r}_1-\mathbf{r}_2|)|V - U_i|\phi_j^{\rm OA}(\mathbf{r}_2)\chi_i^+(\mathbf{r}_1)\rangle. \quad (3)$$

In Eqs. (2) and (3), $\mathbf{r}_1,\mathbf{r}_2$ are the coordinates of the incident and bound electrons, respectively, χ_i,χ_a, and χ_b are the distorted waves for the incident, scattered, and ejected electrons, respectively, $\phi_j^{\rm OA}$ is the OAMO (Ref. 23) for the initial bound state of the molecule generated from molecular orbitals calculated using GAMESS,[27] V is the initial state interaction between the projectile and the neutral molecule, and U_i is the initial state spherically symmetric distorting potential which is used to calculate the initial state distorted wave χ_i. The $C_{\rm proj\text{-}eject}$ term is the Coulomb interaction between the projectile and ejected electron, which allows for postcollision interactions (PCIs).

The molecular distorted waves are calculated using a spherically averaged distorting potential as described in previous work.[19–21] The Schrödinger equation for the incoming electron wave function is given by

$$\left(T + U_i - \frac{k_i^2}{2}\right)\chi_i^+(\mathbf{k}_i,\mathbf{r}) = 0, \quad (4)$$

where T is the kinetic energy operator, $\mathbf{k}_i$ is the initial state wave vector, and the "+" superscript on $\chi_i^+(\mathbf{k}_i,\mathbf{r})$ indicates outgoing wave boundary conditions. The initial state distorting potential $U_i = U_S + U_E$, where U_S is the initial state spheri-

cally symmetric static potential, and U_E is the Furness-McCarthy[24] exchange potential which approximates the effect of the continuum electron exchanging with the passive bound electrons in the molecule. U_E depends on the molecular charge density and is given by

$$U_E = -\tfrac{1}{2}\{(k_i^2 - U_S) - \sqrt{(k_i^2 - U_S)^2 + 2\rho_S(r)}\}. \quad (5)$$

Here $\rho_S(r)$ is the spherically averaged molecular electronic charge density. The radial charge density is defined such that the integral over r yields the number of electrons in the molecule.

The two final channel distorted waves are obtained from a Schrödinger equation similar to Eq. (4):

$$\left(T + U_I + U_E - \frac{k_{a(b)}^2}{2}\right)\chi_{a(b)}^{-}(\mathbf{k}_{a(b)},\mathbf{r}) = 0. \quad (6)$$

Here U_I is the spherically symmetric static distorting potential for the molecular ion which is calculated using the same procedure as U_S, except that the active electron is removed from the charge distribution. The "−" superscript indicates incoming wave boundary conditions.

The details of the DWIAOA molecular orbital are contained in Ref. 19 so only a brief outline will be given here. We start with the PWIA FDCS of Weigold and McCarthy[28]

$$\frac{d^5\sigma}{d\Omega_a d\Omega_b dE_b d\Omega_R} = \frac{4}{(2\pi)^5}\frac{k_a k_b}{k_i}F(\mathbf{k}_i,\mathbf{k}_a,\mathbf{k}_b)\sigma^{\mathrm{PWIA}}(\mathbf{R}), \quad (7)$$

where

$$\sigma^{\mathrm{PWIA}}(\mathbf{R}) = \left|\int d\mathbf{r}\beta_a^*(\mathbf{k}_a,\mathbf{r})\beta_b^*(\mathbf{k}_b,\mathbf{r})\beta_i(\mathbf{k}_i,\mathbf{r})\phi_i(\mathbf{r},\mathbf{R})\right|^2. \quad (8)$$

In Eqs. (7) and (8), $F(\mathbf{k}_i,\mathbf{k}_a,\mathbf{k}_b)$ is an elementary function of the momenta of the incident $(\mathbf{k}_i)$, scattered $(\mathbf{k}_a)$, and ejected electrons $(\mathbf{k}_b)$, respectively.[28] The functions $\beta_i(\mathbf{k}_i,\mathbf{r}), \beta_a(\mathbf{k}_a,\mathbf{r})$, and $\beta_b(\mathbf{k}_b,\mathbf{r})$ are plane waves for the incident, scattered, and ejected electrons, and $\phi_i(\mathbf{r},\mathbf{R})$ is the molecular orbital for the active electron with $\mathbf{R}$ the internuclear vector.

The PWIA is a high energy approximation and fails for lower energy electrons that cannot be approximated by plane waves. For lower energy electrons, we proposed the DWIAOA,[19,21] in which the plane waves of Eq. (8) are replaced by molecular distorted waves and the original molecular orbital is replaced by an OAMO. Using these approximations, Eq. (8) becomes

$$\sigma^{\mathrm{DWIAOA}} = \left|\int d\mathbf{r}\chi_a^{-*}(\mathbf{k}_a,\mathbf{r})\chi_b^{-*}(\mathbf{k}_b,\mathbf{r})\chi_i^{+}(\mathbf{k}_i,\mathbf{r})\phi_i^{\mathrm{OA}}(\mathbf{r})\right|^2, \quad (9)$$

where $\chi_i(\mathbf{k}_i,\mathbf{r})$, $\chi_a(\mathbf{k}_a,\mathbf{r})$, and $\chi_b(\mathbf{k}_b,\mathbf{r})$ are the molecular distorted waves of Eqs. (4) and (6), and $\phi_i^{\mathrm{OA}}(\mathbf{r})$ is the orientation average molecular orbital[23] used in M3DW.

III. EXPERIMENT

The experimental apparatus in which these measurements were performed has been well documented in the literature[3,29–32] and so will only briefly be described here. The $(e,2e)$ spectrometer is fully computer controlled and computer optimized, allowing measurements to be obtained continuously while maintaining optimum operating conditions throughout data collection. The spectrometer is located in a large vacuum chamber which is constructed of nonmagnetic stainless steel lined externally and internally with μ-metal to reduce magnetic fields to <1 mG at the interaction region. All parts of the spectrometer and chamber are constructed of non-magnetic materials, including molybdenum, 310 stainless steel, copper, polytetrafluroethylene (PTFE), and polyetheretherketone (PEEK). The base pressure of the chamber is around 1×10^{-7} torr, whereas during operation this pressure is maintained at 1×10^{-5} torr due to the target hydrogen gas effusing from a hypodermic needle through the interaction region and into the chamber. A 500 l/s turbo molecular pump backed by a 15 l/s rotary pump evacuates the chamber during operation.

The spectrometer consists of an energy unselected electron gun, which produces an ~1 mm diameter electron beam at the interaction region over a range of energies. The gun uses a Pierce grid and anode to efficiently extract electrons from a tungsten filament (the cathode). The resulting electrons are then directed to the interaction region using two electrostatic lenses which are separated by a field free region in which 1 mm diameter pencil and beam angle defining apertures are located. The gun is designed to produce zero beam angle at the interaction region with a small pencil angle controlled by the finite size of the defining apertures.

The electron gun produces a nominal 1 mm diameter beam at the interaction region, the physical size of this beam varying slowly with incident energy due to the effects of focusing of the lenses, and space charge in the electron beam. For the experiments detailed here, it is assumed that the electron beam has a diameter of 1 mm, which is a reasonable estimate given the high electron energy and relatively low electron beam currents that were adopted. Direct tests of the physical size of the electron beam were not possible in this apparatus; however, independent checks of the size of the interaction region have been made by observing fluorescence from the electron excited target using a well focused photomultiplier tube.[29] These tests confirm that the measured electron beam dimensions correspond to the calculated size, particularly at high energies.

By ensuring that the incident electron energy remained constant throughout the measurements presented here, variations due to refocusing of the electron gun as in previous coplanar symmetric studies from H_2 (Ref. 3) were eliminated. This allows confidence to be assigned to the relative measurements presented here.

Although the incident electron beam remained constant at 75.3 eV throughout data collection, the detected electron energies varied from 2 to 58 eV, so as to ensure energy conservation between the scattered and ejected electrons from

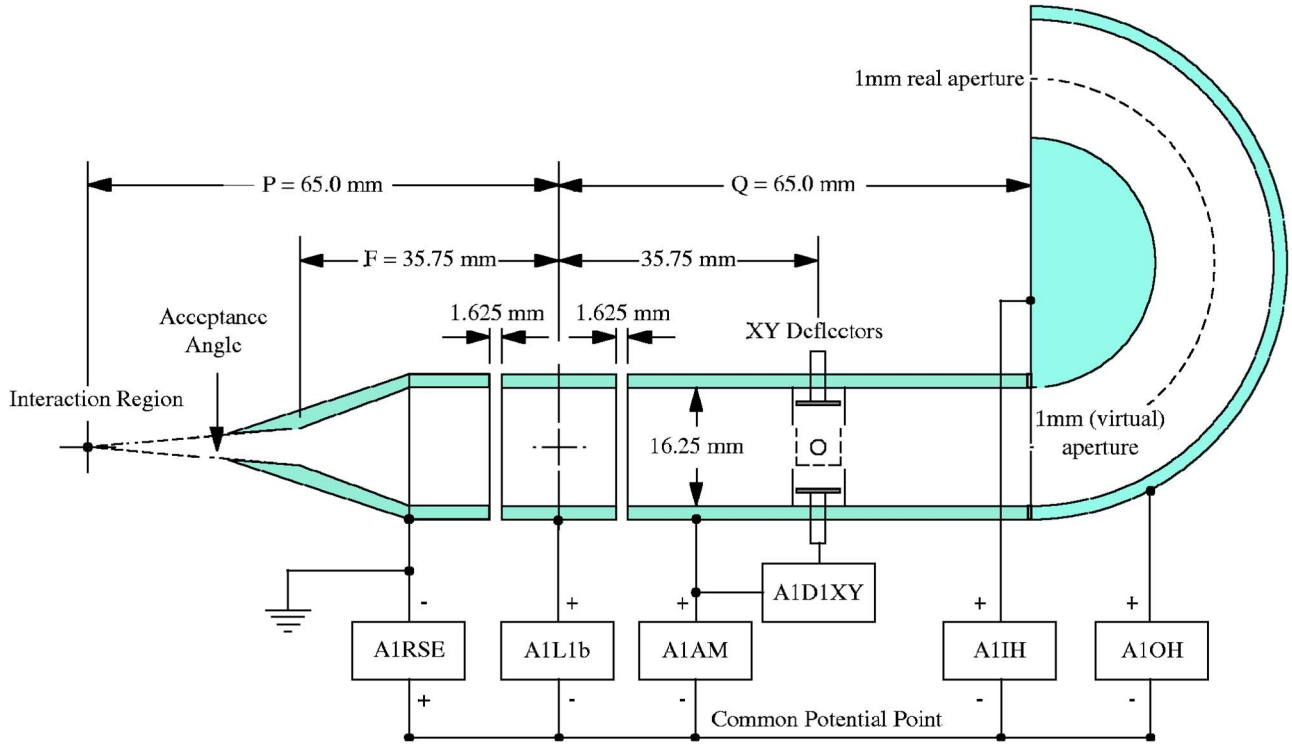

FIG. 2. The analyzer lens used in the $(e,2e)$ spectrometer in Manchester, shown to scale. The interaction region is imaged onto a 1 mm virtual aperture produced by the hemispherical energy analyzer from the real output aperture. The distance between the interaction region and defining aperture is 130 mm, so that $P=Q=4D$, where D is the lens diameter. The gap between lenses is set to 0.1 D. The arrangement of the power supplies for the electrostatic lens is shown and is described in the text.

the ionization process. To allow for this variation in energy, the electrostatic lenses used in the detectors were modeled using SIMION (Ref. 33) to estimate the efficiency of detection for each energy. The analyzers used in the spectrometer are identical in construction, and so it was only necessary to model a single analyzer to estimate the total efficiency, taking the product of efficiencies for each analyzer to determine overall losses.

Figure 2 details the electron analyzers used in the spectrometer at Manchester. Energy selection is implemented using a hemispherical energy selector which has second order focusing and an effective magnification of unity. A 1 mm real aperture at the output of the selector is therefore mapped as a 1 mm virtual aperture at the input to the selector. Jost correctors[34] are used at the input and output to minimize the effects of field distortions inside the hemispheres. A Photonis X719BL channel electron multiplier (CEM) detects and amplifies the electrons which emerge from the output aperture, so that electrons that pass through this aperture are counted.

The input lens to the analyzer consists of a three-stage electrostatic cylindrical lens which allows the two analyzers to closely approach each other without colliding. The input to the lens is conically shaped and is held at earth potential (0 V reference to the interaction region), so that electrons from the interaction region travel without deviation into the analyzer. The acceptance angle of the analyzer is defined by the size of the input aperture and the distance between the aperture and interaction region as shown.

Lens focusing is controlled by applying a potential to element A1L1b so that a maximum signal is detected by the CEM following energy selection. A pair of electrostatic deflectors allows for small imperfections in the lenses. The potential of these deflectors is referenced symmetrically around the potential of the field free region A1AM so that the electrons are deflected rather than focused by these elements.

All parts of the electron analyzers are constructed of molybdenum, which is completely nonmagnetic and which has been found to be an excellent material for electron optical systems used at low energies. The energy analyzer hemispheres are also spun from molybdenum and are isolated from the lens using small sapphire balls. The spacing between the lenses is accurately set using machined spacers, which are then removed so that these spaces are in vacuum. No insulating materials are therefore located within the analyzer lenses or selectors, ensuring the effects of insulator charging, which can be detrimental to the operation of the analyzer, are eliminated.

The potentials for the analyzers are set as shown in Fig. 2. Selection of the residual energy of the electrons which are passed to the CEM detector is set by adjusting A1RSE to the correct voltage (e.g., 50 eV electrons are passed by setting A1RSE to 50 V). All lens elements and energy selecting elements are then referenced to this potential. The pass energy of the electrons which travel around the energy selector is set by adjusting the potential of lens element A1AM, which was set to 10 eV throughout data collection. The potentials of the inner and outer hemispheres were then adjusted to ensure that only 10 ± 0.3 eV electrons were detected by the CEM,

TABLE I. Calculated normalized efficiencies of the analyzer lens as a function of residual energy.

Residual Energy (eV)	Efficiency
58	0.51±0.02
55	0.52±0.02
50	0.54±0.02
40	0.60±0.01
30	0.72±0.01
2	0.94±0.01
5	1.00±0.01
10	0.95±0.01
20	0.85±0.01
30	0.72±0.01

using power supplies A1OH and A1IH, these potentials remaining constant with respect to the residual energy throughout the experiment.

By ensuring that the pass energy of the electrons was always set to 10 eV, only one potential (A1L1b) is required to image electrons from the interaction region into the CEM detector (ignoring deflector voltages, which to a good approximation do not focus the electrons). The electrostatic lens therefore acts as a zoom lens, and as such will have a variable efficiency for detection of electrons from the interaction region. This efficiency can be estimated using a model of the lens which solves Laplace's equation for the potentials inside the lens, and then determines the trajectories of the electrons which succeed in entering the energy analyzer.

The model used for this analysis was SIMION, which solves Laplace's equation using a finite element analysis to derive the potentials on a fine grid.[33] This model assumes cylindrical symmetry on a two dimensional (2D) grid, which is a reasonable approximation since the lenses are also cylindrical in shape. The 1 mm interaction region was modeled as 25 individual points on a 2D grid, each point being used as the source of electrons directed into the analyzer. Fifty different electron trajectories were launched from each point at each electron energy, so as to cover the range of angles which could enter the analyzer input aperture. The experimentally determined voltages for the analyzer lens elements were then used to set up the potentials in the model, and the efficiency of detection was determined by counting the number of electron trajectories that successfully passed through a 1 mm defining aperture located in the position of the virtual aperture shown in Fig. 2. The lens efficiency was then estimated by taking the ratio of electrons entering the lens to that which successfully passed through the 1 mm aperture.

Table I shows the efficiency of the lens as a function of residual energy, as estimated from the model. The results are normalized to unity for a residual energy of 5 eV. Results for each 2D point in the interaction region were weighted according to the volume element which they represent in three dimensions, assuming a cylindrical symmetry. This weighting also requires that the electron density and target density in the interaction region are uniform over the interaction volume, which is reasonable given the small interaction volume. The uncertainty in the lens efficiency was estimated by determining the fraction of electrons entering the defining aperture compared with those that just collided with the surface of the aperture.

TABLE II. Renormalized product of efficiencies for the combined analyzer lenses.

Energy (E_a,E_b) (eV)	Efficiency
58, 2	0.91±0.04
55, 5	1.00±0.03
50, 10	0.98±0.02
40, 20	0.97±0.02
30, 30	0.99±0.02
20, 40	0.97±0.02
10, 50	0.98±0.02

Although the normalized efficiency of the analyzer lenses varied significantly from 0.51 (58 eV electrons) to 1.0 (5 eV electrons) as shown in Table I, these differences tend to cancel out for the $(e,2e)$ coincidence signal, as shown in Table II. In this table, the efficiency of detection of pairs of electrons in coincidence is estimated from the product of efficiencies for each analyzer, renormalized to unity at residual energies of 55 eV for the fixed analyzer and 5 eV for the moving analyzer. The largest variation occurs for the combination of lenses detecting 58 and 2 eV electrons, where a loss of 10% in the signal is expected compared to results at 55 eV/5 eV. For all other lens combinations, the relative variation in efficiency compared to 55 eV/5 eV detection is less than 5%.

The losses estimated from the model presented in Table II were used to renormalize the experimental data prior to comparing the results to the theoretical calculations described in Sec. II. The results of these comparisons are detailed in the next section.

The coincidence technique adopted in the experiments uses standard high speed components for timing resolution. Signals from the electron detectors in each analyzer were amplified using Philips Scientific 100× preamplifiers before being passed directly to Ortec 473A constant fraction discriminators (CFDs). The discriminators produced (NIM) nuclear instrument module compatible output pulses to an Ortec time to amplitude converter (TAC) which was connected to an Ortec multichannel analyzer (MCA). One of the electron signals from the CFD was delayed prior to entering the stop input of the TAC, so that the time correlated signal from the detectors appeared centrally in the MCA window.

The correlated event signal was derived from the MCA signal by subtracting the background due to uncorrelated events in the usual way. The angular cross section was then determined from the correlated event signal by moving the analyzer around the detection plane as shown in Fig. 1, with data being accumulated at each scattering angle for a set period of time.

IV. RESULTS AND ANALYSIS

As depicted in Fig. 1, a coplanar asymmetric geometry was chosen for these studies where the incident electron energy was set to 75.3 eV, and one of the analyzers was fixed

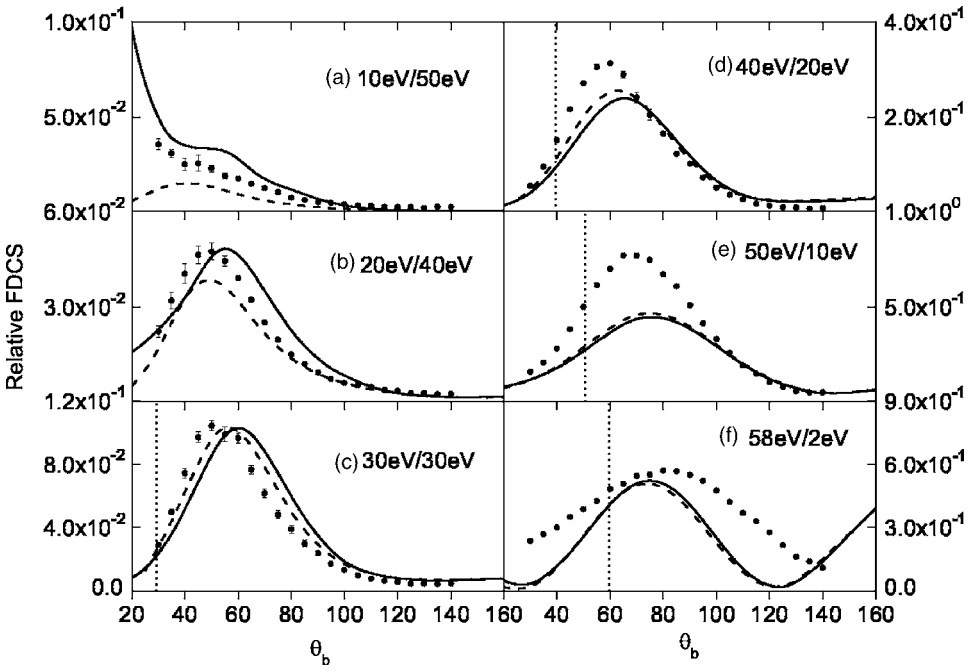

FIG. 3. Experimental and theoretical fully differential cross section (FDCS) results for 75.3 eV electron-impact ionization of H_2 in coplanar asymmetric geometry. One final state electron is observed at a fixed scattering angle $\theta_a=22°$ and the scattering angle for the other electron θ_b varies from 30° to 140°. The different parts of the figure correspond to different pairs of energies E_a/E_b for the two final state electrons. The black circles with error bars are the experimental data, solid lines are M3DW results including the exchange amplitude but excluding the Furness-McCarthy exchange potential, and dashed lines are M3DW results without the exchange amplitude and without the Furness-McCarthy exchange potential. The vertical dotted straight lines indicate the classical momentum transfer direction.

at a forward scattering angle $\theta_a=22°$. The second electron analyzer located on the opposite side of the interaction plane detected electrons at angles varying from $\theta_b=30°$ to $\theta_b=140°$, allowing the binary peak in the cross section to be determined. The electron energies varied from $(E_a,E_b)=(10\text{ eV},50\text{ eV})$ through $(20\text{ eV},40\text{ eV})$, $(30\text{ eV},30\text{ eV})$, $(40\text{ eV},20\text{ eV})$, $(50\text{ eV},10\text{ eV})$, and $(58\text{ eV},2\text{ eV})$. The count rates for the detected electrons varied widely, from a maximum count rate of ~30 kHz to a rate of <1 kHz, depending on the scattering angle and energy. The electron beam current was set to ~200 nA for data collection so as to optimize the coincidence rate while ensuring that the detector efficiency remained in a linear regime, and the pressure in the vacuum chamber was held constant at 10^{-5} torr. Data were collected for 3000 s at each angle around the scattering plane, ranging by 5° intervals from $\theta_b=30°$ to $\theta_b=140°$. Up to ten full sweeps of the scattering plane were conducted to establish the shape of the cross section and to determine the statistical uncertainty in the measurements. An uncertainty of ±3° was estimated for the angles based on the acceptance angle of the analyzers, and the pencil angle of the incident electron beam.

Figures 3–5 show the normalized experimental results together with calculations using the M3DW and DWIAOA theoretical models. Only a single relative normalization point was chosen between theory and experiment for all measurements which are shown, as discussed above. In each figure, the theoretical results are normalized to the experimental peak value for $(E_a,E_b)=(30\text{ eV},30\text{ eV})$.

In previous work by the authors,[18] only the direct ampli-

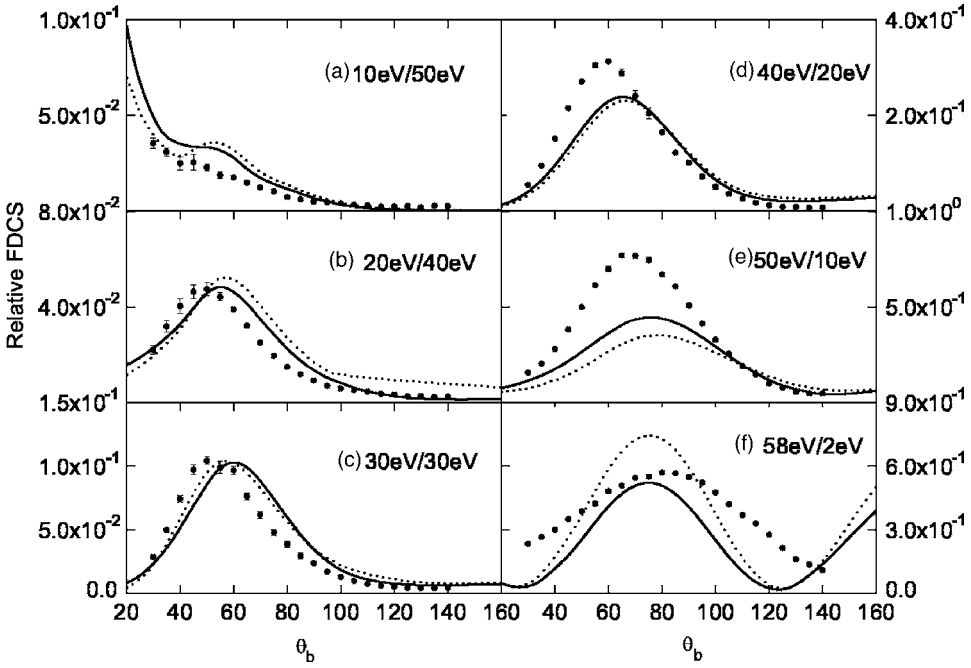

FIG. 4. Same as Fig. 3. Here the solid lines are M3DW results including the exchange amplitude but excluding the Furness-McCarthy exchange potential, and dotted lines are M3DW results including the exchange amplitude and the Furness-McCarthy exchange potential.

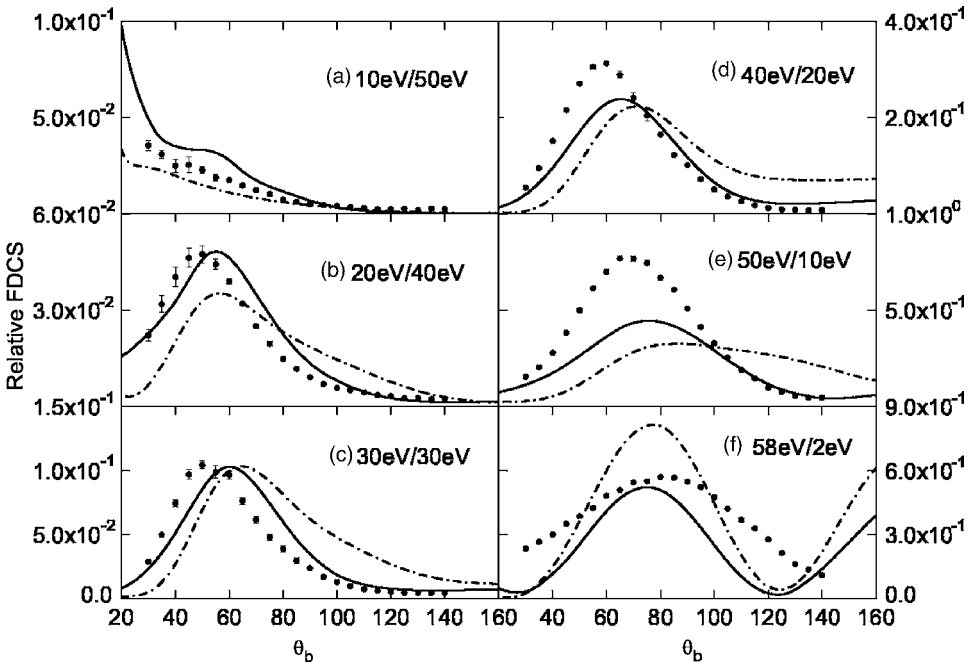

FIG. 5. Same as Fig. 3. Here the solid lines are M3DW results including the exchange amplitude but excluding the Furness-McCarthy exchange potential, and the dashed-dotted lines are DWIAOA results.

tude for the cross section was calculated, which is appropriate for symmetric scattering or highly asymmetric scattering processes. Since the exchange amplitude may be important for the kinematic conditions of the experiments detailed here, we first examine the importance of the exchange amplitude. In Fig. 3, the solid lines show the M3DW results with both direct and exchange amplitudes included, and the dashed lines represent results where only the direct amplitude is included. In the calculations for the direct amplitude, the projectile is observed at $\theta_a=22°$, whereas in the exchange amplitude the ejected electron is observed at $\theta_a=22°$. For this case, one would expect that the direct amplitude should dominate the 58 eV/2 eV results of case (f). As can be seen from Fig. 3, exchange becomes more important with decreasing energy for the fixed electron detector and becomes the dominant effect for 10 eV/50 eV as expected. However, it is surprising to note that exchange appears to be relatively unimportant for the intermediate energy cases. For highly asymmetric collisions, the binary peak is normally located near the direction of momentum transfer of the projectile to the molecule. The straight dotted lines shown in Fig. 3 show the direction of momentum change between the projectile and the electron observed in the fixed detector at $\theta_a=22°$. For parts (a) and (b) of Fig. 3, the classical momentum transfer directions are at $\theta=11.6°$ and $\theta=20.1°$, respectively, so they are not observable in the angular range of the figure. As can be seen from Fig. 3, the momentum transfer direction approaches the binary peak as the energy of the fixed electron increases. However, for lower energy electrons in the fixed detector, the "binary peak" is far from the momentum transfer direction and for the lowest energy case of part (a), there is only a hint of a peak in the experimental data and M3DW results with exchange. This is a direct observation of the fact that the classical collision model is applicable only when the incident electron does not lose much energy.

The exchange amplitude takes into account exchange between the two continuum electrons. Another quantum mechanical exchange effect is exchange between the continuum electrons and one of the bound target electrons. To properly include this exchange effect would require a Hartree-Fock calculation of the continuum electron wave function, which is not practical at this point. The local potential approximation of Furness-McCarthy has been shown to yield reasonably accurate results for atomic ionization.[25,26] In Fig. 4, the solid lines are M3DW results without using the Furness-McCarthy exchange potential, and the dashed lines are results which include the Furness-McCarthy exchange potential. Both the direct and exchange amplitudes have been used in these calculations. For ionization of atoms, it is known that exchange between the continuum electrons and a bound electron is most important for lower energy continuum electrons, and we see this expected effect in Fig. 4. In contrast with atomic ionization, the Furness-McCarthy potential does not improve agreement between experiment and theory. Consequently, this approximation is probably not appropriate for molecules such as H_2.

Distorted wave impulse approximation calculations were also performed with the orientation averaged (DWIAOA) wave function, to test the accuracy of this simplified approximation. In Fig. 5, DWIAOA and M3DW results are compared with the experimental measurements. In previous work,[18] it was found that the DWIAOA was reasonably accurate for higher energy coplanar asymmetric collisions. For the present asymmetric scattering case, the DWIAOA is clearly not as good as the M3DW, except for the 10 eV/50 eV data of part (a). This is particularly intriguing since, from Fig. 3, it was seen that the small angle increase in the cross section for the 10 eV/50 eV case results from the exchange amplitude and that the direct amplitude only had a binary peak near 40°. In the DWIAOA model there is no distinction between direct and exchange amplitudes, and it yields the best agreement with experiment when exchange is

most important. More testing of this approximation is necessary to determine if these results are important or just fortuitous in this case.

V. CONCLUSIONS

Relatively normalized experimental results for 75.3 eV electron-impact ionization of H_2 have been compared with different theoretical calculations in coplanar asymmetric scattering geometry. Pretty good agreement has been found between experiment and the M3DW results when both direct and exchange amplitudes are included in the calculation.

Exchange between the continuum electrons and the bound electrons has also been found to be important for low energy continuum electrons. However, it appears that the local potential approximation of Furness and McCarthy which has been useful for ionization of atoms will not be valid for ionization of molecules.

An additional effect which is likely to be important is polarization of the molecular charge cloud. The importance of polarization has recently been investigated,[18,19] using an *ad hoc* polarization potential which has an adjustable cutoff radius. For coplanar symmetric ionization of H_2, this polarization potential was found to improve agreement between experiment and theory using a cutoff radius of $1.5a_0$. When the same parameters were used for the present kinematics, the agreement between theory and experiment became worse. Since we do not like adjustable parameters, it was decided not to pursue this type of polarization potential further. In the future it is hoped to incorporate a parameter free polarization potential such as the one proposed by Nesbet.[35]

The agreement between experimental results and the *ab initio* theoretical models found in the present studies is encouraging, as it implies that much of the physics of the interaction is being included. The experiments still suffer from several limitations, which need to be addressed for the most rigorous comparison to be made to theory. It is becoming increasingly important to determine *absolute* cross sections from the data so that the magnitude of the cross sections can be established accurately. Of equal importance is to achieve alignment of the molecular axis with respect to the scattering geometry, so that averaging over the direction of the molecules as carried out in the theoretical analysis described above becomes unnecessary. Both of these goals are difficult to achieve experimentally; however, they would provide the most rigorous tests of theory for ionization of these molecular systems.

ACKNOWLEDGMENTS

The support of the NSF under Grant No. PHY-0456528 is gratefully acknowledged. The EPSRC is also acknowledged for providing support for the experimental program described here.

[1] K. T. Leung and C. E. Brion, J. Electron Spectrosc. Relat. Phenom. **35**, 327 (1985).
[2] D. S. Milne-Brownlie, S. J. Cavanagh, B. Lohmann, C. Champion, P. A. Hervieux, and J. Hanssen, Phys. Rev. A **69**, 032701 (2004).
[3] A. J. Murray, J. Phys. B **38**, 1999 (2005).
[4] I. N. Levine, *Quantum Chemistry*, 5th ed. (Prentice-Hall, Upper Saddle River, NJ, 2000).
[5] R. S. Mulliken and W. C. Ermler, *Diatomic Molecules: Results of Ab Initio Calculations* (Academic, New York, 1977).
[6] T. E. McCarthy, J. Phys. B **6**, 2358 (1973).
[7] E. Weigold, S. T. Hood, I. E. McCarthy, and P. J. O. Teubner, Phys. Lett. **44A** 531 (1973).
[8] S. Dey, I. E. McCarthy, P. J. O. Teubner, and E. Weigold, Phys. Rev. Lett. **34**, 782 (1975).
[9] E. Weigold, I. E. McCarthy, A. J. Dixon, and S. Dey, Chem. Phys. Lett. **47**, 209 (1977).
[10] B. Van Wingerden, J. T. K. Kimman, M. Van Tilburg, and F. J. de Heer, J. Phys. B **14**, 2475 (1981).
[11] J. N. Migdall, M. A. Coplan, D. S. Hench, J. H. Moor, J. A. Tossell, V. H. Smith, and J. W. Liu, Chem. Phys. **57**, 141 (1981).
[12] K. T. Leung and C. E. Brion, Chem. Phys. **82**, 113 (1983).
[13] M. Chérid, A. Lahmam-Bennani, A. Duguet, R. W. Zurales, R. R. Lucchese, M. C. Dal Cappello, and C. Dal Cappello, J. Phys. B **22**, 3483 (1989).
[14] F. Robicheaux, J. Phys. B **29**, 779 (1996).
[15] A. L. Monzani, L. E. Machado, M. T. Lee, and A. M. Machado, Phys. Rev. A **60**, R21 (1999).
[16] P. Weck, O. A. Fojon, J. Hannsen, B. Joulakian, and R. D. Rivarola, Phys. Rev. A **63**, 042709 (2001).
[17] C. R. Stia, O. A. Fojón, P. F. Weck, J. Hanssen, B. Joulakian, and R. D. Rivarola, Phys. Rev. A **66**, 052709 (2002).
[18] J. Gao, D. H. Madison, and J. L. Peacher, J. Phys. B **39**, 1275 (2006).
[19] J. Gao, D. H. Madison, and J. L. Peacher, Phys. Rev. A **72**, 020701(R) (2005).
[20] J. Gao, J. L. Peacher, and D. H. Madison, AIP Conf. Proc. **811**, 72 (2006).
[21] J. Gao, D. H. Madison, and J. L. Peacher, Phys. Rev. A **72**, 032721 (2005).
[22] J. Gao, D. H. Madison, and J. L. Peacher, J. Chem. Phys. **123**, 204314 (2005).
[23] J. Gao, J. L. Peacher, and D. H. Madison, J. Chem. Phys. **123**, 204302 (2005).
[24] J. B. Furness and I. E. McCarthy, J. Phys. B **6**, 2280 (1973).
[25] D. H. Madison, V. D. Kratsov, and S. Mazevet, J. Phys. B **31**, L17 (1998).
[26] C. Mette, T. Simon, C. Herting, G. F. Hanne, and D. H. Madison, J. Phys. B **31**, 4689 (1998).
[27] M. W. Schmidt, K. K. Baldridge, J. A. Boats *et al.*, J. Comput. Chem. **14**, 1347 (1993).
[28] E. Weigold and I. E. McCarthy, *Electron Momentum Spectroscopy* (Kluwer Academic, New York, 1999).
[29] A. J. Murray, B. C. H. Turton, and F. H. Read, Rev. Sci. Instrum. **63**, 3346 (1992).
[30] A. J. Murray, Phys. Rev. A **72**, 062711 (2005).
[31] A. J. Murray and D. Cvejanovic, J. Phys. B **36**, 4875 (2003).
[32] M. J. Hussey and A. J. Murray, J. Phys. B **38**, 2965 (2005).
[33] SIMION modeling software, www.simion.com
[34] K. Jost, J. Phys. E **12**, 1001 (1979).
[35] R. K. Nesbet, Phys. Rev. A **62**, 040701(R) (2000).